ISSN 0038-0946, Solar System Research, 2007, Vol. 41, No. 6, pp. 447–462. © Pleiades Publishing, Inc., 2007.
Original Russian Text © V.V. Shevchenko, V.I. Chikmachev, S.G. Pugacheva, 2007, published in Astronomicheskii Vestnik, 2007, Vol. 41, No. 6, pp. 483–489.

Structure of the South Pole–Aitken Lunar Basin

V. V. Shevchenko, V. I. Chikmachev, and S. G. Pugacheva

Sternberg State Astronomical Institute, Lomonosov Moscow State University, Universitetskii pr. 13, Moscow, 119899 Russia

Received April 10, 2007

Abstract—The hypsometric map and the basin height profiles, for the first time relying upon a spherical daturence surface, have been constructed based on the generalization of the heights measured within the hemisphere including the ring structure of the South Pole–Aitken basin. The distribution of the major chemical elements (Fe and Th), depending upon the structure height levels, has been obtained. The relationship between these lunar rock indicators and the height levels of the rock preferential distribution has been revealed. The outer basin ring has been distinguished and the ring structure of the central basin depression has been revealed against a combined hypsometric and geochemical background. A total basin diameter of about 3500 km has been reliably determined for the first time. A unique feature of the basin structure consists in that the arrangement of the basin inner rings does not show a central circular symmetry, which can indicate that a hypothetical impactor moved along the trajectory (or orbit) oriented almost normally to the ecliptic plane. In combination with the revealed very small depth–diameter ratio in the initial basin structure, this circumstance makes it possible to put forward the hypothesis that a comet impact produced the South Pole–Aitken basin.

DOI: 10.1134/S0038094607060019

INTRODUCTION

The nature and origin of a unique formation, which is still conditionally called the South Pole–Aitken basin, remain one of the most important problems in recent studies of the Moon. The basin, which apparently belongs to the pre-Imbrian Period, is the largest ring formation not only on the lunar surface, but also in the entire Solar System. Not only the basin dimensions on an absolute scale but also the fact that the basin diameter almost coincides with the lunar diameter are of interest. A similar relationship is not observed on other silicate or icy bodies in the Solar System.

The diameter (1300 km) of one of the largest partially studied ring formations in the Solar System—the Caloris Planitia on Mercury (Pike and Spudis, 1987)—is about 0.27 the planet diameter. According to preliminary estimates, the largest ring structure on Mercury, supposedly located in the hemisphere not studied based on the *Mariner-10* spacecraft images, has a relative diameter of 0.48 (Ksanfomality, 2004). The generalized relationship between the relative diameter of the largest ring structures and the radius of the corresponding bodies in the Solar System was derived by Shevchenko et al. (1985).

The Valhalla ring formation on Callisto has a relative diameter similar to the diameter of the South Pole–Aitken basin. However, the structure of this basin considerably differs from that of South Pole–Aitken, first of all, in that the Valhalla basin does not have such a deep central depression as that observed on the lunar analog. The problem was studied in detail by Hiesinger and Head (2004), who arrived at the conclusion that the above structures are of different types.

This feature of the giant lunar basin immediately attracted special attention, because it became hypothetically possible to reveal rock samples from the lower crustal layers or even the upper mantle among ancient ejecta. Wilhelms (1987), Spudis (1993), Spudis et al. (1994), and Petro and Pieters (2004, 2006) assumed that 43–45 impact basins of more than 300-km in diameter had formed during the first ~700 Myr of the Moon's existence as a celestial body. This process favored the excavation and distribution of rock fragments from the lunar crust's deep layers over the lunar surface. It seems even more probable to identify and study similar samples within or in the vicinity of the South Pole–Aitken basin using remote or direct methods, since this formation is among the most ancient and largest structures; the bottom zones of this formation should be the deepest.

At the same time, previous detailed studies of the structure of the South Pole–Aitken basin cannot be considered complete, and several problems of the structure and genesis of this unique formation should be further studied.

THE SOUTH POLE–AITKEN MULTIRING BASIN

The history of the discovery of the largest planetary ring structure and the initial stages in the study of this structure were described by Chikmachev and Shevchenko (1999).

It was preliminarily estimated that this structure originated about 4 Ga ago (Petro and Pieters, 2002). During the subsequent period, the modification of the ring structure itself and the superposition of numerous

Table

References	Outer ring diameter, km	Coordinates of the outer ring center	
		longitude, deg	latitude, deg
Stuart-Alexander (1978)	2000	180	50 S
Wilhelms et al. (1979)	2500	180	56 S
Wood and Gifford (1980)	2600	180	60 S
Leikin and Sanovich (1985)	2200	176.5 E	41.5 S
Petro and Pieters (2002)	–	170 E	56 S
Hiesinger and Head (2004)	2400	174 W	55 S

younger impact craters considerably distorted the initial shape of the South Pole–Aitken (SPA) basin. Therefore, it becomes difficult to identify the basin boundaries by means of the geological deciphering based on the background topography. Most direct morphological features of the initial structure rings were completely or almost completely destroyed during later crater formations.

The table illustrates the differences in determining the outer ring diameter and coordinates of the geometric center of this ring caused by difficulties in identifying the topographical boundaries of this formation.

After several epochs of destructive crater bombardment, the boundaries of highlands, ranges, and basin slopes have become smoothed and diffused.

Even the most-perfect examples of geological deciphering yield indistinct results in this respect (Hiesinger and Head, 2004).

As a result of the performed preliminary analysis, we have come to the conclusion that it is necessary to construct a generalized topographic macromodel of the southern polar region of the Moon in order to reveal the true contours of the SPA basin multiring structure (Chikmachev and Shevchenko, 1999). The first significant result in this direction was the discovery of the basin outer ring itself, the dimensions of which proved to be more considerable than the estimates by other authors (table). Chikmachev et al. (2005) initiated this new stage of study.

A structural analysis of the SPA basin was based on the hypsometric map of the hemisphere including this basin. The map was constructed in the perspective azimuthal orthographic projection (Fig. 1). The results of Clementine laser altimetry (Spudis et al., 1994), the catalogs of the absolute elevations of the far side of the Moon were obtained based on the *Zond* survey materials (Rodionov et al., 1976; Chikmachev, 1983, 1986; Kislyuk, 1988; Kaula et al., 1973), and the results of ground-based studies of the lunar limb relief (Nefed'ev, 1958) were the initial data used to construct the hypsometric map shown in Fig. 1. A standard daturence surface with a radius of 1738 km was used to count off heights. The technique for constructing the generalized hypsometric model using the above data was published in Chikmachev and Shevchenko (1999).

Based on the assumption of a circular symmetry of the basin with respect to the profiles crossing the formation in perpendicular directions, we determined the coordinates of the depression outer ring center: $\lambda = 180°$, $\beta = -40° (\pm 2°)$. Figure 2 shows the position of the profiles in the map projection: (*1*) and (*2*) are the positions of the height profiles obtained based on the limbs from the *Apollo-11* and *Zond-8* images, respectively; and (*3*) and (*4*) are the positions of the height profiles constructed based on the data of the *Apollo-16* and *Apollo-15* laser altimeters, respectively.

The hypsometric map shown in Fig. 1 makes it possible to study the generalized structure of the SPA basin relief. The basin outer ring is traced based on the system of highlands in the northwestern, northern, northeastern, and eastern zones of the ring structure. Figure 3 presents the generalized topographic profile of the considered hemisphere along the 180° meridian (*1*). The spherical daturence surface is shown by segment (*2*). The maximal altitude of the outer ring crest in its northern zone is marked by (*a*). The deepest part of the basin inner depression is denoted by (*b*). The vertical and horizontal scales of the profile are identical. The basin profile constructed for the first time based on the spherical daturence surface demonstrates the real depth–diameter ratio for the basin.

In Fig. 4, the vertical scale of the same profile is increased by a factor of 20, so that it is possible to trace the relief details. The basin central depression, which is located asymmetrically relative to the outer ring of the highlands and is evidently shifted southward in the deepest zone of the basin, is distinctly traced on the profile.

PRESENT-DAY STRUCTURE AND DIMENSIONS OF THE SPA BASIN OUTER RING

To reveal the outer ring structure, we constructed a 3D topographic model, the heights of which exceed the zero level, using the data from the hypsometric map (Fig. 1). This model is presented in Fig. 5 in the perspective projection. To identify the position of the distinguished structure on the lunar surface, we indicated in Fig. 5 the morphological features corresponding to a number of large formations on the Moon. For obvious reasons, we increased the vertical scale of the constructed model compared to the linear scale. The perspective azimuthal orthographic projection, identical to the hypsometric map projection shown in Fig. 1, is the horizontal background for the model. The model rect-

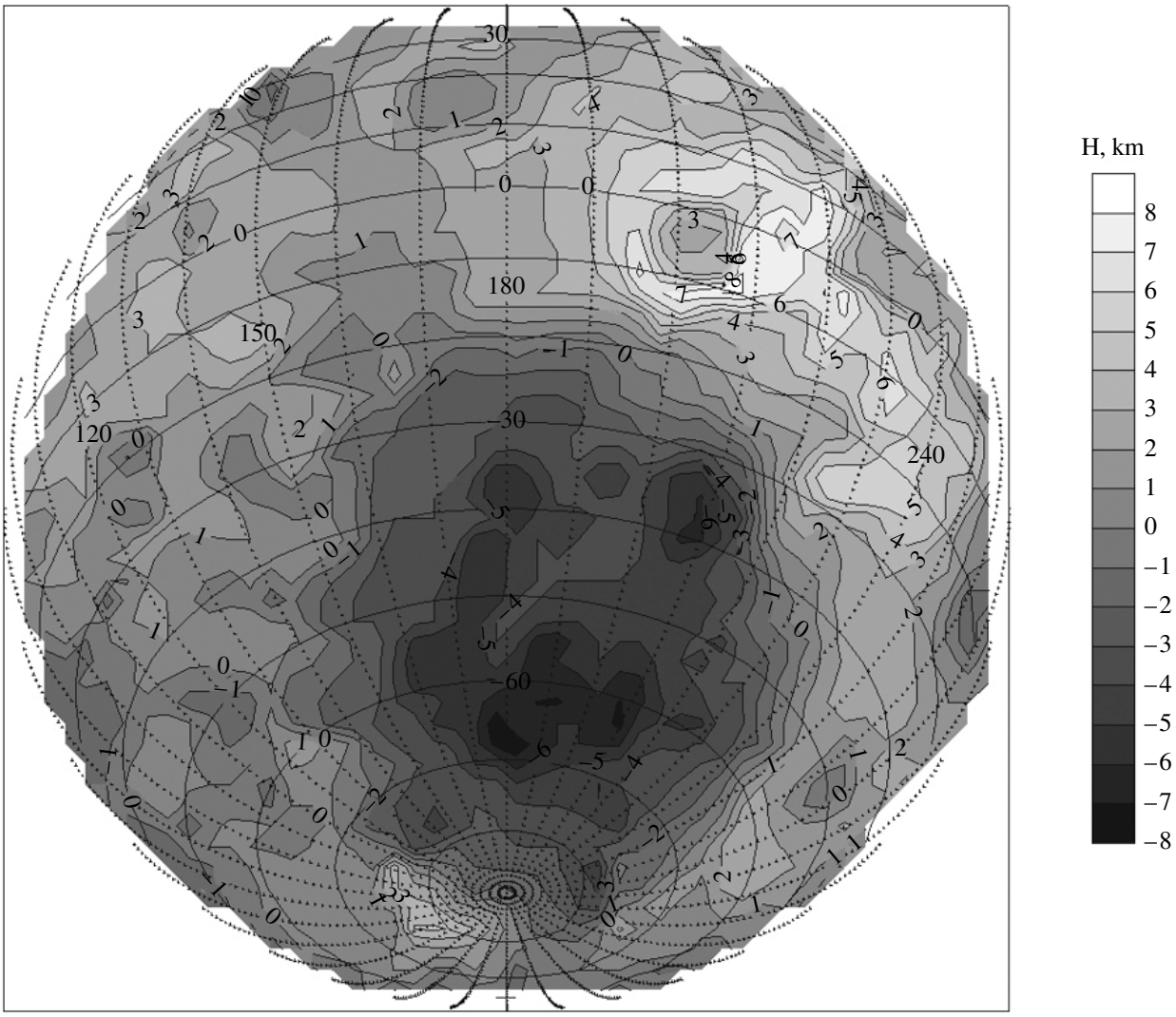

Fig. 1. The hypsometric map of the lunar hemisphere including the SPA basin. The map was constructed in the perspective azimuthal orthographic projection. The initial data and construction method are described in the text.

angular grid is oriented in the north–south and west–east directions. The mesh angular dimensions are 0.5° × 0.5°, which corresponds to 15 × 15 km for the sides of the squares oriented along the central meridian. The latitudinal linear dimensions of the square sides vary in a standard way depending on the position of each mesh.

The main conclusion drawn based on an analysis of the topographic model presented in Fig. 5 consists in that the distinguished ring of positive topographic features corresponds to the position and dimensions of the initial outer ring of the SPA basin complex structure with a high probability. The formations are most intact in the northwestern and northeastern ring segments (northward direction at the top of Fig. 5). The formation crest between the Tsiolkovskiy crater and the southern margin of the Mare Moscoviense depression reaches a height of about +3 km at the most elevated zone. The northeastern segment includes crest zones with heights of up to +7–8 km in the region extending from the Korolev crater to the western margin of the Mare Orientale inner depression. Figure 6 demonstrates the vertical profile in the azimuthal direction of 45° from the accepted structure center to the margin of the assumed outer ring. The profile of the elevated area is of special interest. In this direction, the ring of the positive topographic features is more than 1700-km-wide at heights reaching 6–7 km from the datum level in the central zone. We can assume that this segment is the most intact zone of the basin outer ring.

It is interesting that the outer ring generally has the shape of an embankment rising above the background surface level.

At present, the southwestern ring segment is almost not observed, which is possibly related to the destruction and degradation of the relief caused by the later formation of the Mare Australe depression.

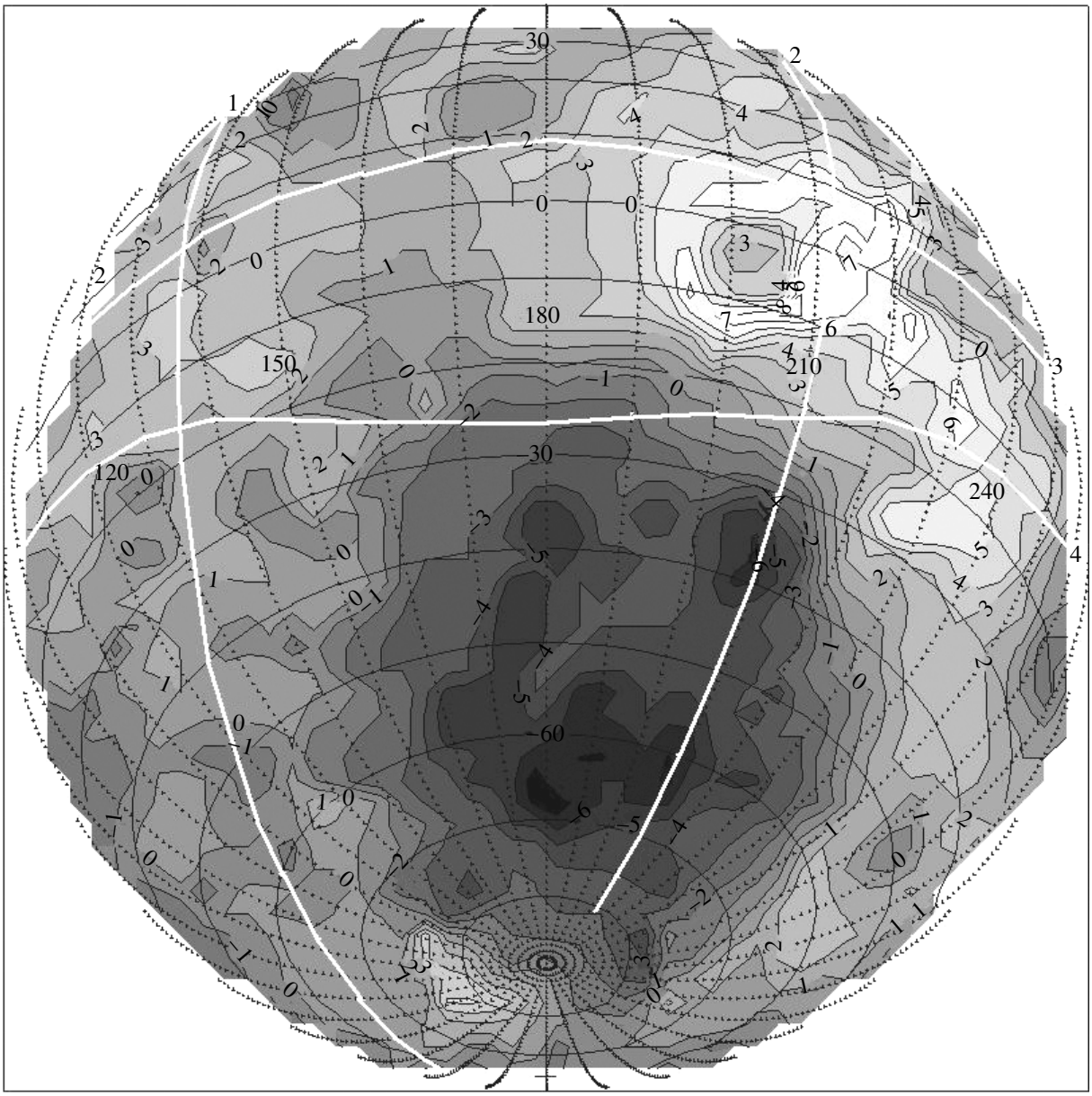

Fig. 2. The center of the basin outer ring based on the height profiles of the projections, which are indicated on the map: (*1*) and (*2*) are the projections of the visible disk limbs from the *Apollo-11* and *Zond-8* images, respectively; (*3*) and (*4*) are the projections of the height profile obtained along the *Apollo-16* and *Apollo-15* orbits, respectively.

The destruction of the initial ring relief in the southeastern segment can be related to the formation of several large craters, such as Bailly, Mendel–Rydberg complex, and others. The Mendel and Rydberg craters form one large depression on the hypsometric map. Hiesinger and Head (2004) also combined these objects into one structure when they analyzed the morphology of the SPA basin. The inner ring boundary drawn by these researchers (including the northern, eastern, and southern ring zones) almost coincides with the inner contours of similar segments of the structure distinguished in Fig. 5 by means of a hypsometric analysis.

In spite of the fact that the main part of the southern segment of the initial outer ring of the SPA basin proved to be almost completely destroyed, the basin boundaries in this region can be marked owing to such a relic formation as Malapert Mountain. The Malapert Mountain summit has an elevation of +4.5 km, which is unambiguously typical of the most intact northeastern segment of the outer ring. According to the images of the summit and its surroundings shown in Fig. 7, the surface of this formation demonstrates that this structure belongs to an ancient continental landscape typical of other distinguished segments of the SPA basin outer ring. Malapert Mountain and the topographical features

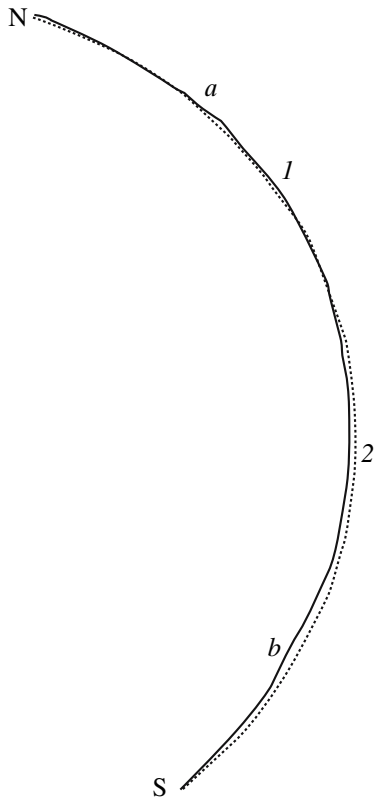

Fig. 3. The height profile along the *180* meridian constructed based on the hypsometric map data. North is at the top, (*1*) is the surface profile, (*2*) is the spherical daturence surface, (*a*) is the crest of the northern segment of the basin outer ring, and (*b*) is the deepest zone of the inner depression. The vertical and horizontal scales of the profile are identical.

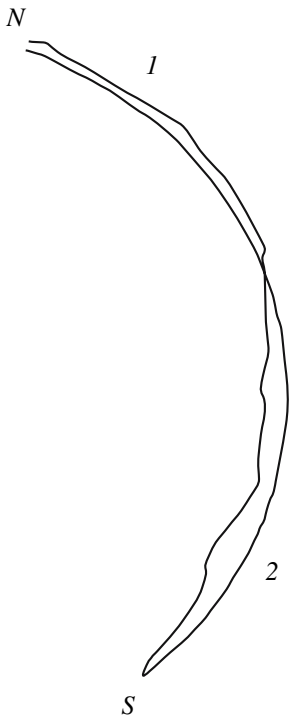

Fig. 4. The height profile along the 180° meridian constructed based on the hypsometric map data. North is at the top, (*1*) is the surface profile, and (*2*) is the spherical daturence surface. The scale of profile *1* for the absolute elevations is increased by a factor of 20 compared to the linear scale of the distances on the spherical surface.

in immediate proximity to this formation are shown in two areas distinguished on the central image (the left-hand inset). The lower right-hand image shows the character of the relief in the central zone of the northeastern segment of the surviving outer ring. The coordinates of the center of this zone are 240° E and 40.5° S. The left-hand inset is 151.5 × 136.3 km at an original resolution of about 100 m per pixel. The right-hand inset is 90 × 90 km at a resolution of 64 m per pixel. The lower right-hand image has the same dimensions at an original resolution of about 100 m per pixel. The images presented in Fig. 7 evidently illustrate the ancient continental landscape and show that the landscapes are of the same character in both cases as compared to the relief of the surviving segment of the basin outer ring.

A comparison of the surface rock chemistry in the Malapert Mountain region and in the northeastern zone of the outer ring is an additional argument for a similar conclusion.

Figure 8 presents the map of the iron content distribution within the considered hemisphere constructed based on the Lunar Prospector gamma-ray spectrometer measurements. The catalog of iron content measurements converted to a unit area of 0.5° × 0.5° was used as the initial data (Lawrence et al., 1998, 2002; Prospector, 2006). The map was constructed in a projection identical to the projection of the hypsometric map shown in Fig. 1.

An analysis of the map presented in Fig. 8 indicates that the iron abundance within the outer ring varies from 3.0 to 4.0 wt %. The iron content of the surface rocks in the Malapert Mountain region quite agrees with these values (3.0–3.5 wt %). According to the same Lunar Prospector measurements, the titanium (0.2–0.3 wt %) and thorium (1.5–2.0 ppm) contents of the surface rocks in the Malapert Mountain region are unambiguously similar to the content of surface rocks in other segments of the basin outer ring previously determined (Lucey et al., 1998).

To make a general comparison, we can indicate that the Malapert Mountain rocks are similar to typical continental rocks at the *Apollo-16* moon-landing site in terms of the abundance of the above elements. The average abundance of iron, titanium, and thorium in the samples delivered to Earth were about 3.88 and 0.3 wt % and 0.43–3.7 ppm, respectively (Haskin and Warren, 1995).

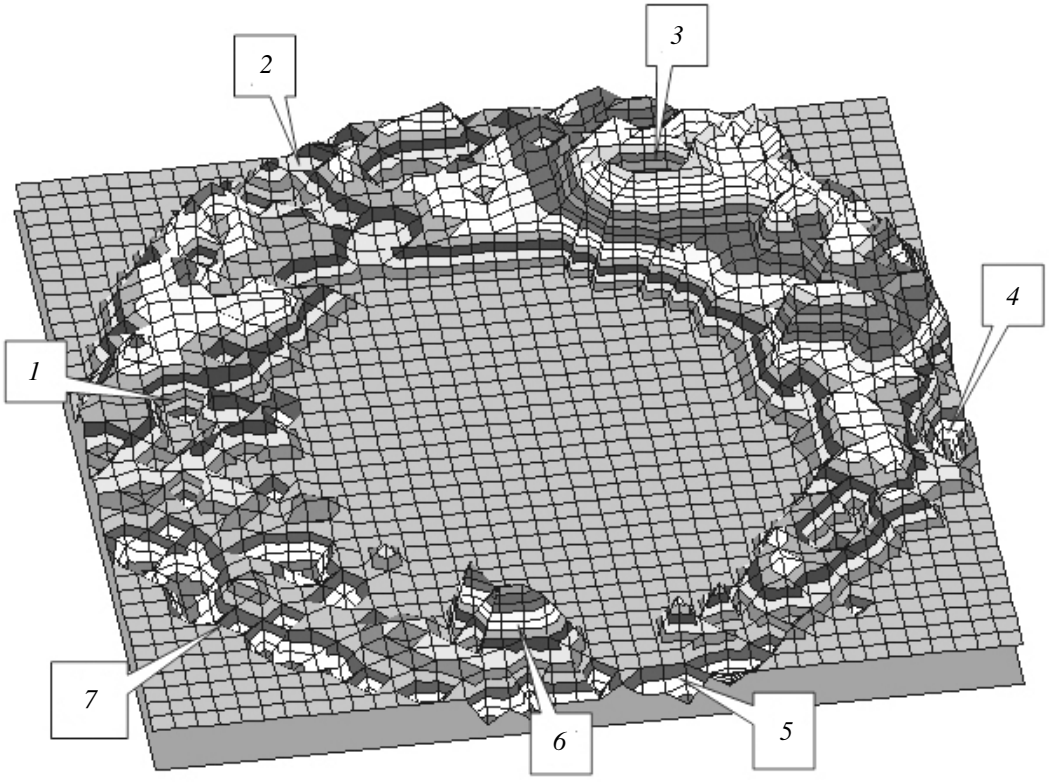

Fig. 5. The structure of the SPA basin outer ring (the 3D projection). The position of certain topographic features of the lunar surface is marked on the image: (*1*) Tsiolkovskiy crater, (*2*) the Mare Moscovience margin, (*3*) the Korolev basin, (*4*) part of the Mare Orientale central depression, (*5*) the Bailly crater margin, (*6*) Malapert Mountain, and (*7*) the eastern boundary of the Mare Australe depression. The relief is shown relative to the daturence surface corresponding to a sphere with a radius of 1738 km. The contour lines are drawn at an interval of 0.5 km. The vertical scale is increased compared to the linear scale. The hypsometric structure of the SPA inner depression is not indicated.

Thus, such a relic formation as Malapert Mountain can probably be related to the general structure of the SPA outer ring in its original form.

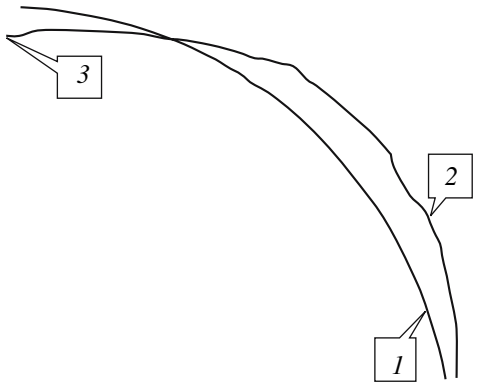

Fig. 6. The height profile in the azimuthal direction of 45° counted off from the northern part of the map at the central meridian in Fig. 1 with a longitude of 180°. (*1*) The spherical daturence surface corresponding to a sphere with a radius of 1738 km; (*2*) the height profile of the vertical scale, which is increased by a factor of 20; and (*3*) the point of the selected center of the ring structure.

Assuming that the initial structure of the SPA basin outer ring is circularly symmetric, we can estimate the general dimensions of this uniquely giant lunar formation. If we take the median zone of the extensive ridges in the northern and northeastern segments of the ring structure as a conditional outer boundary of the formation, the average structure diameter is equal to 3500 km. If we take the distance from the center to the Malapert Mountain summit as the radius, the general dimensions of the basin outer ring will be even larger. However, in this case, we cannot be sure that this relic formation exactly delineates the initial structure boundary according to the definition presented above.

STRUCTURE OF THE SPA BASIN CENTRAL DEPRESSION

In spite of the fact that the general height difference in the SPA basin exceeds 16 km, the primary depth penetration of this structure is relatively insignificant, taking into account that the formation diameter is huge (see the profiles in Figs. 3 and 4). The basin structure has substantially changed as a result of the intense impact transformation of the surface over several bil-

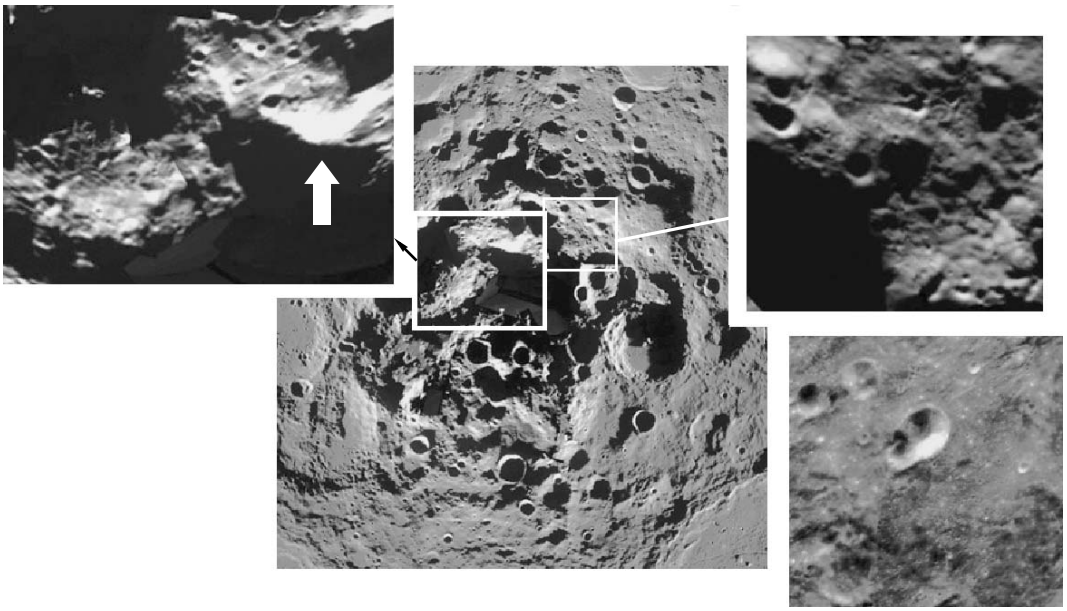

Fig. 7. Fragments of the mosaic compiled using the *Clementine* images (the southern polar region). Malapert Mountain is marked by an arrow on the left-hand inset. The description is given in the text. The central image, left-hand inset, and lower right-hand insets are NASA–USGS photographs. The right-hand upper inset is an ESA–SMART image.

lion years; however, this transformation did not delete certain traces of the initial basin formation (Peterson et al., 2002). Wieczorek and Phillips (1999) and Hiesinger and Head (2004) hold the same opinion.

Since the inner depression of the SPA basin was not filled with lava, this formation is the only ancient lunar structure for which the primary excavation depth is close to the currently observed depth and does not require special reconstruction. A uniquely small depth–diameter ratio for the SPA basin is confirmed by comparing it to similar characteristics of the largest ring formations on the Moon. In Wieczorek and Phillips (1999), which was the final work for a cycle of studies by these researchers in this direction, it was indicated that the depth–diameter ratio for the SPA basin is an order of magnitude as small as the value determined by extrapolating a similar dependence for ring structures larger than 200 km when compared with the diameter of the depression that originated during the excavation stage.

A comparison of the considered characteristics on the absolute scale of magnitudes quite definitively indicates that the SPA basin structure is unique, and the depth–diameter ratio does not result in a dependence typical of other basins observed on the Moon. Figure 9 demonstrates the dependence of the reconstructed excavation depth on the diameter of the corresponding depression from the data presented in Wieczorek and Phillips (1999) for the formations of 200–500 km in diameter (*1*). The SPA basin, for which the depression diameter during the excavation stage was taken equal to 2099 km at an excavation depth of 17.6 km, occupies position (*2*) on the diagram. According to our version, the excavation depth and the diameter of the corresponding depression can be taken as equal to 14 and 2575 km, respectively, based on the hypsometric map shown in Fig. 1 and the profiles presented in Figs. 4 and 6. In this case, the SPA basin will occupy position (*3*) on the diagram in Fig. 9.

In spite of a certain difference in the positions of (*2*) and (*3*) due to differences in the outer ring diameter accepted in either case, it is quite evident that the SPA formation does not correspond to the general tendency for large lunar ring formations with respect to the above parameters and is characterized by an anomalously shallow depth at a considerable diameter.

Numerous remote studies of the surface material performed within the basin and in immediate proximity to the basin indicate that the rocks of the initial impact melting account for no less than 15% of the present-day surface regolith (Petro and Pieters, 2004). This material, in which norite together with mafic rocks predominate according to the spectral data, possibly represents matter from the lower crust and upper mantle of the Moon exposed during the basin formation and partially remelted during primary impact and in the process of subsequent cratering within the SPA basin (Jolliff et al., 2002).

In particular, Jolliff and Gillis (2005) emphasized that an analysis of the abyssal rock chemistry in the SPA basin, based on the data on the iron and thorium abundances, can make it possible to solve such key problems as the KREEP-rich rock distribution in the middle and lower crust and the determination of the relationship between mafic materials, including rocks

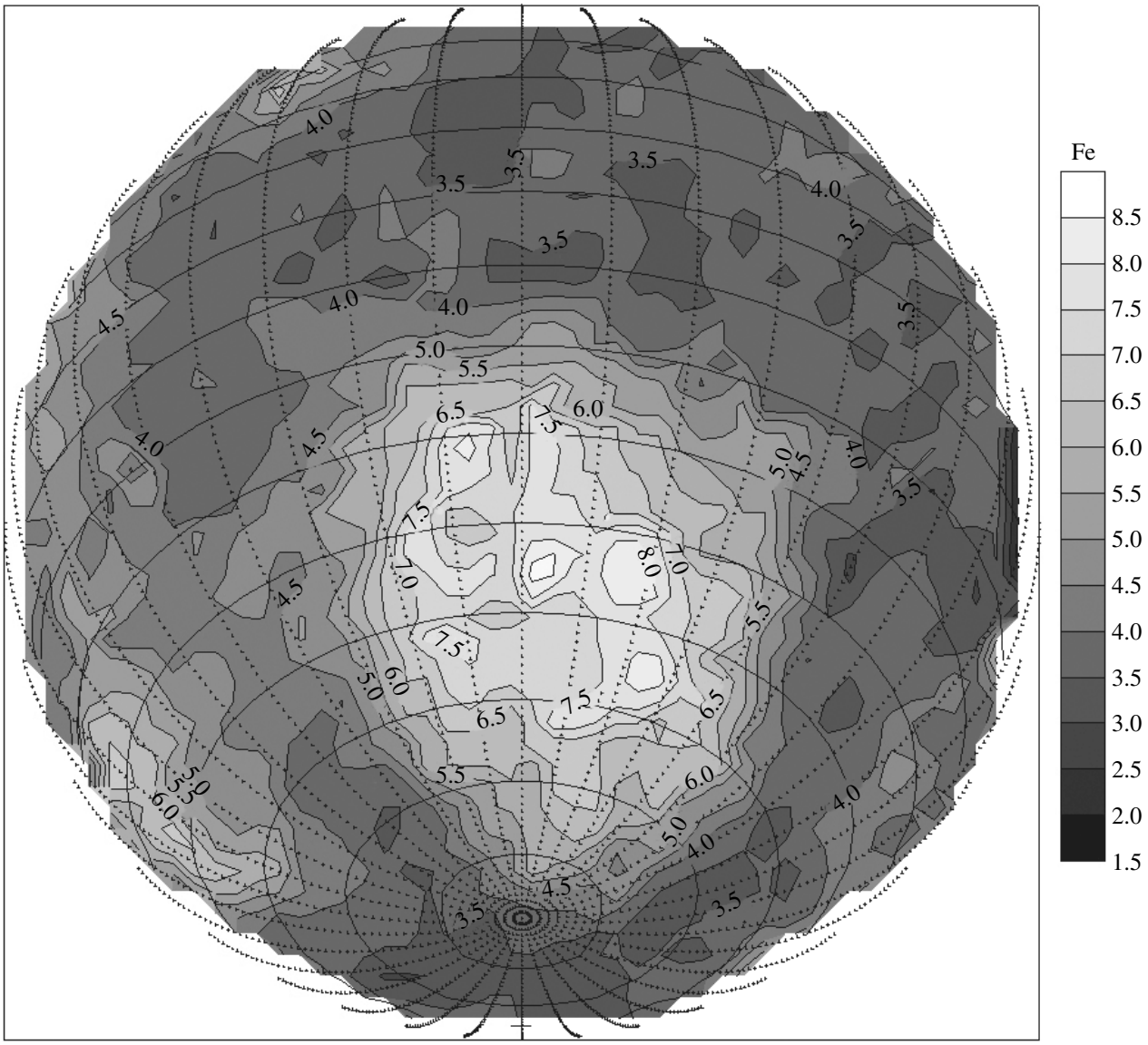

Fig. 8. The iron content distribution within the SPA basin. The map was constructed in a projection similar to the hypsometric map projection (Fig. 1).

enriched in iron or magnesium, in the upper and lower crusts.

In the present work, we tried to more specifically trace the material chemistry at different levels within the studied ring structure based on the iron and thorium abundances. A preliminary analysis of the data indicated that the dependence of the chemistry on the depth for the SPA basin is very generalized and takes the form of a cluster with very blurred boundaries on the corresponding diagram. Therefore, to reveal the boundary abundances of individual chemical elements (in this case, those of iron and thorium) depending on depth horizons, we selected a method for analyzing marginal distributions successfully used in a number of studies (see, e.g., Jolliff et al., 2002; Lawrence et al., 2003).

Figure 10 presents the iron content distribution in the surface layer of the SPA basin, corresponding to the entire formation (distribution *5*) and to different height levels (distributions *1–4*). The presented plots were constructed based of a statistical analysis of the data shown on the iron content map (Fig. 8). Except for distributions *1* and *4*, the remaining distributions have bi- (distributions *2* and *3*) and trimodal (distribution *5*) forms. The separation of marginal distributions indicates that the first mode, which is identical for distributions *3–5* and represents an iron content equal to ~3.5%, characterizes the rocks at levels higher than 0 km. According to the geochemical estimates, these rocks are of the anorthosite type (Haskin and Warren, 1995; Peterson et al., 2002). The second mode sepa-

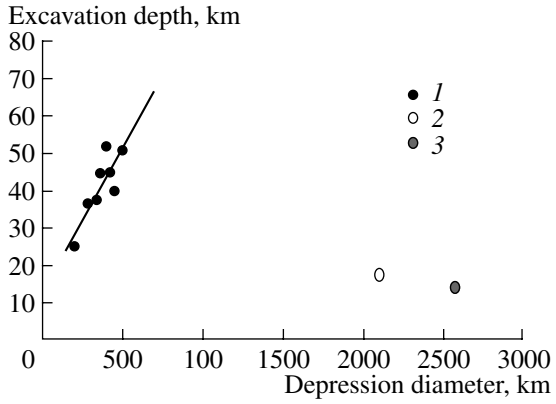

Fig. 9. The excavation depth depending on the excavation depression diameter: (*1*) the dependence for the ring structures 200-500-km in diameter according to Wieczorek and Phillips (1999); (*2*) the position of the SPA basin according to the data of the same researchers; and (*3*) the position of the SPA basin according to the data obtained in the present work.

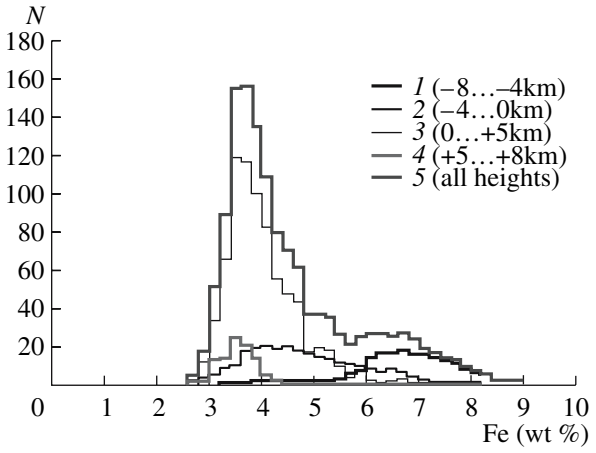

Fig. 10. The iron content distributions in the surface layer at different heights of the SPA basin structure.

rated in distributions *2*, *3*, and *5* corresponds to an iron abundance of ~4.5%. Finally, the third mode separated in distributions *1–3* and *5* characterizes an iron abundance of ~6.5%.

The distributions characterizing the correspondence of the iron content to different height levels for the SPA basin inner depression are distinguished in Fig. 11. A comparison of these marginal distributions indicates that the second mode separated in distributions *2* and *3* corresponds to an iron abundance of ~4.5%. Finally, the third mode separated in distributions *1–3* characterizes an iron content equal to ~6.5%.

An analysis of the described marginal distributions indicates that the first boundary level, i.e., the boundary between the first and second distributions (~4% Fe), corresponds to a height of 0 km as compared to the hypsometric map shown in Fig. 1. Similarly, the boundary between the second and third distributions (~5.5% Fe) corresponds to a height of –4 km.

Taking into account that the performed analysis is based on the combined characteristics of the SPA basin central depression, a substantial feature of the rock composition can be the abundance of thorium; as is known, the latter indicates that abyssal rocks of the norite type were carried to the surface. Figure 12 presents the map of the thorium abundance distribution within the SPA formation constructed in the perspective azimuthal orthographic projection. The Lunar Prospector measurements were used as the initial data (Lawrence et al., 2002; Prospector, 2006).

Figure 13 demonstrates the thorium distributions for the entire formation (distribution *5*) and for different height levels (distributions *1–4*). An analysis of these polymodal distributions indicates that the first mode, corresponding to a thorium abundance of ~1.25 ppm (distributions *2–4* and *5*), characterizes anorthosite rocks from the SPA basin outer ring. The second mode corresponds to a thorium abundance of ~1.75 ppm (distributions *1–3* and *5*). The third mode is separated when the thorium content is ~2.75 ppm (distributions *1*, *2*, and *5*). Finally, the fourth mode, which reflects a statistically small part of the studied data set, corresponds to a thorium abundance of ~3.75 ppm (distributions *1*, *2*, and *5*).

The marginal distributions, which reflect the variations in the thorium content depending on the depth in the basin inner depression, are distinguished in Fig. 14. By comparing the thorium distribution character with the hypsometric parameters of the SPA basin inner depression, we can make sure that the boundary between the first and second distributions on average corresponds to a height of 0 km (1.5 ppm Th). The boundary between the second and third distributions on average corresponds to a height of –4 km (2.5 ppm Th).

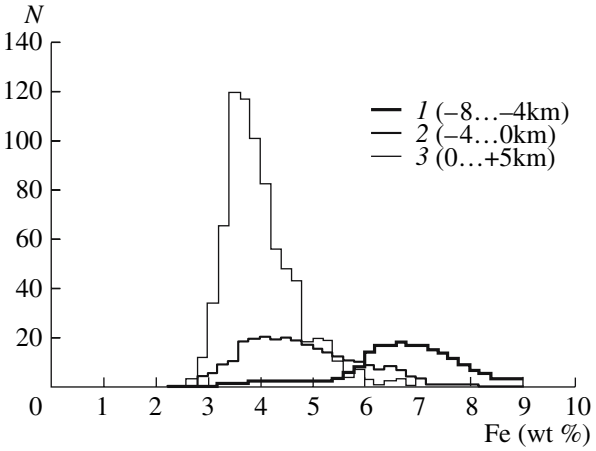

Fig. 11. The iron distributions at different heights in the inner zone of the SPA basin.

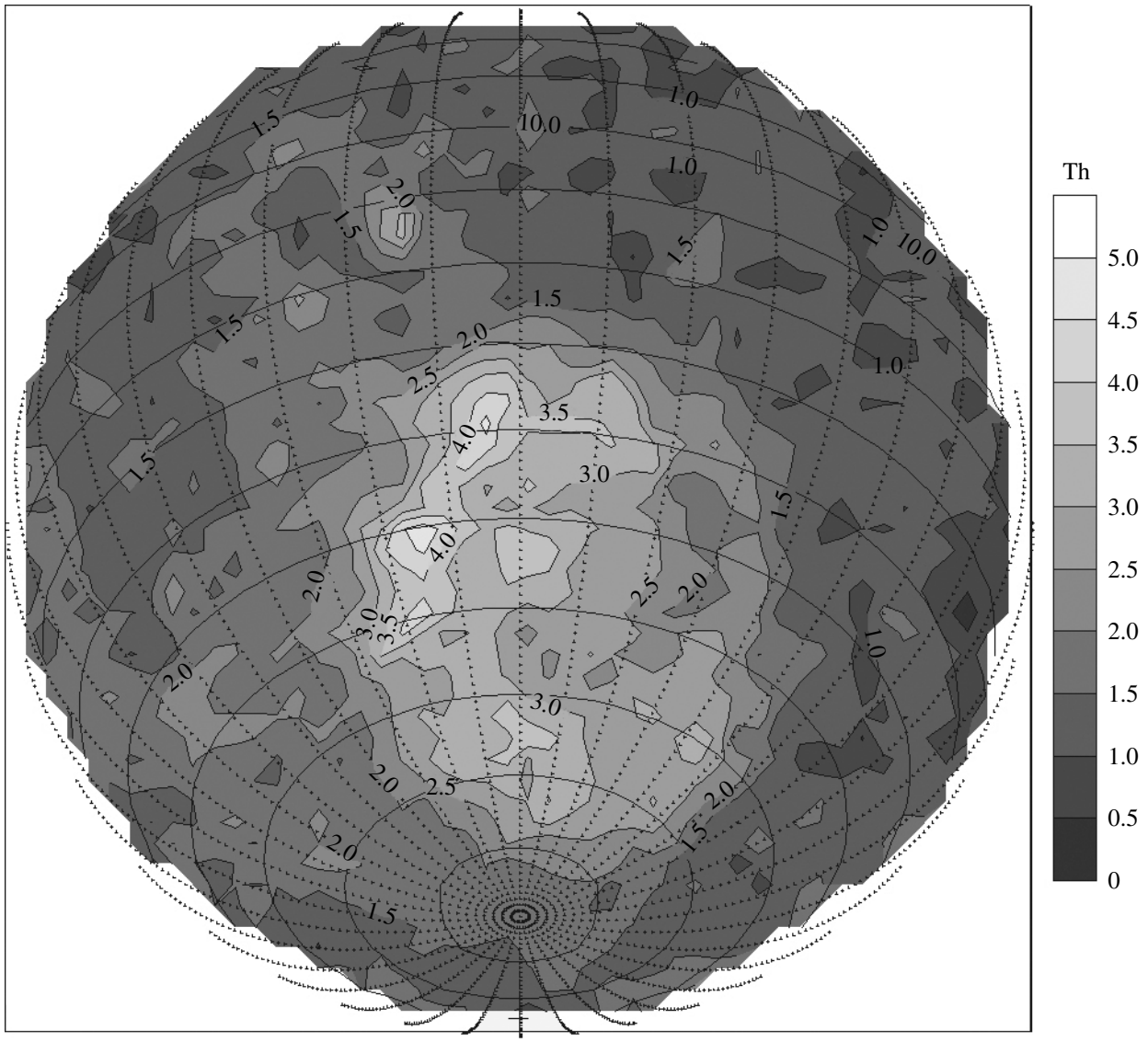

Fig. 12. The thorium content distribution within the SP basin. The map was constructed in a projection similar to the hypsometric map projection (Fig. 1).

A more thorough analysis indicated that the fourth mode (~3.75 ppm Th) shown in Fig. 13 does not correspond to the observed sequence of heights. Different researchers previously assumed that the considered anomaly of the thorium content is the zone of the material carried from outside, i.e., the product of ejecta during the formation of a younger large structure on the Moon (Wieczorek and Zuber, 2001; Garrick-Bethell and Zuber, 2005). In this case, the authors assumed that the revealed anomaly of the surface thorium content could be formed as a result of antipodal ejecta, e.g., during the impact bombardment of the Mare Imbrium basin.

The fact that the thorium content mode separated above does not correlate with the system of ring depressions of the SPA basin can indicate that a similar assumption is reliable.

The histogram shown in Fig. 15 demonstrates the height distribution in the SPA basin region constructed based on the hypsometric data reduced to the map in Fig. 1 at an interval of 0.5 km. According to Fig. 15, the general distribution is polymodal and can be resolved into several marginal distributions in order to reveal the detailed structure of the SPA basin central depression. In a first approximation, we can distinguish three marginal distributions, each of which has a form close to normal. In this case, the first, second, and third modes are about 2, –1, and –5 km, respectively. Accordingly, the boundary between the first and second distributions is located at a height close to 0 km, and the boundary

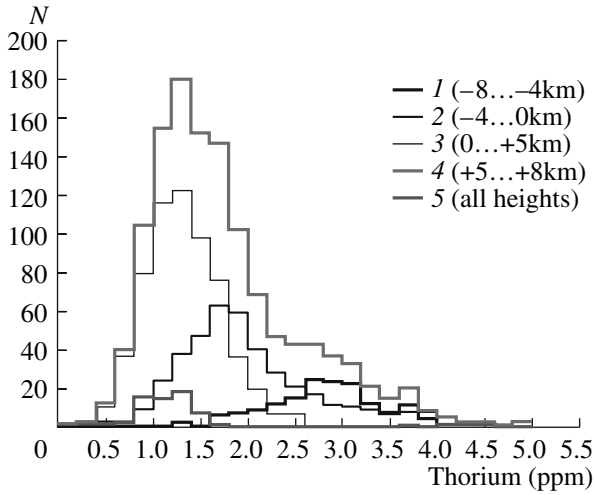

Fig. 13. The thorium distributions in the surface layer at different heights of the SPA basin structure.

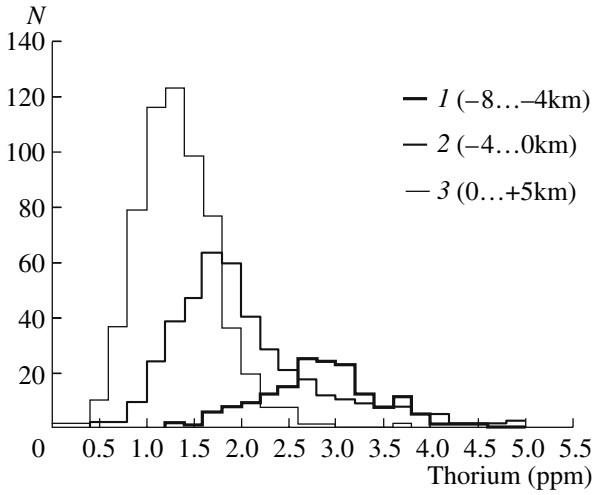

Fig. 14. The thorium distributions in the surface layer at different heights in the inner zone of the SPA basin structure.

between the second and third distributions passes at a height of about –3.5 km.

By comparing these data with the above analysis of iron and thorium vertical distributions, we can conclude that the character of the structures distinguished in both cases is almost identical. Thus, using two independent methods, it was determined that the SPA basin inner depression has two clearly defined height levels (inner rings): less than 0 and –4 km. Based on the hypsometric map (Fig. 1), we can trace one more small depression considerably shifted toward the south of the entire structure, the heights within which are lower than –6 km. This third ring is not distinguished in the height distribution nor in the distribution of the chemical elements, apparently, because of the small ring area. At the same time, this detail is substantial when the general basin structure is analyzed.

MULTIRING STRUCTURE OF THE SPA BASIN

Generalizing the analysis of the SPA basin structure, we can refer to the following specific features of this giant formation (Fig. 16).

Based on the combined analysis of the hypsometric data and rock chemistry at different heights, we constructed the ellipses corresponding to the boundary height values distinguished above and the iron and thorium abundances. Using the Monte-Carlo method, we determined the height boundaries uniformly moving rectangular mesh points. A point was displaced from the center of the region with minimal heights ($H = –8$ km) to the specified height values (H_n). Thus, we distinguished four height rings where the rms deviation is minimal. The calculated statistical parameters of heights within each ring made it possible to determine the shape and dimension of the ring zone heights. It was established that the height zones have relatively simple contours and the shape of ellipses. Circular scattering was observed for a small area (H less than –5 km).

A substantial feature of the scheme shown in Fig. 16 consists in that the hypsometric structures of the distinguished rings are different.

The outer ring marked by O in Fig. 16 coincides with the conditional crest of the elevated zone around the basin (Figs. 5 and 6). Excluding the destroyed segments in the southern zone of the ring, the ring shape can be assumed to be circularly symmetric with an average diameter of about 3500 km counted off from the projection on the daturence surface with a radius of 1738 km. The inner boundary of a wide outer ring passes at a height of about 0 km, which geometrically

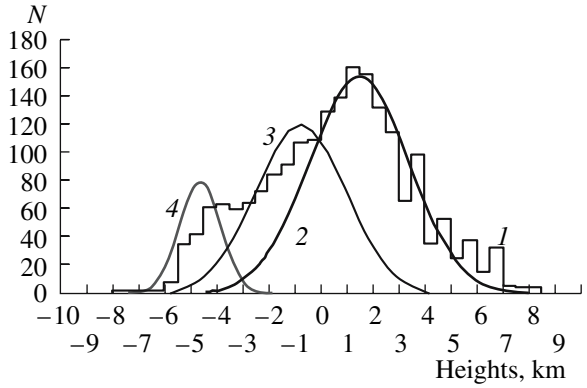

Fig. 15. The height distribution in the SPA basin region constructed according to the hypsometric map data (Fig. 1): (*1*) the height distribution within the entire structure; (*2*) the marginal height distribution within the basin outer ring; (*3*) the marginal height distribution within the first inner ring; and (*4*) the marginal height distribution within the second inner ring.

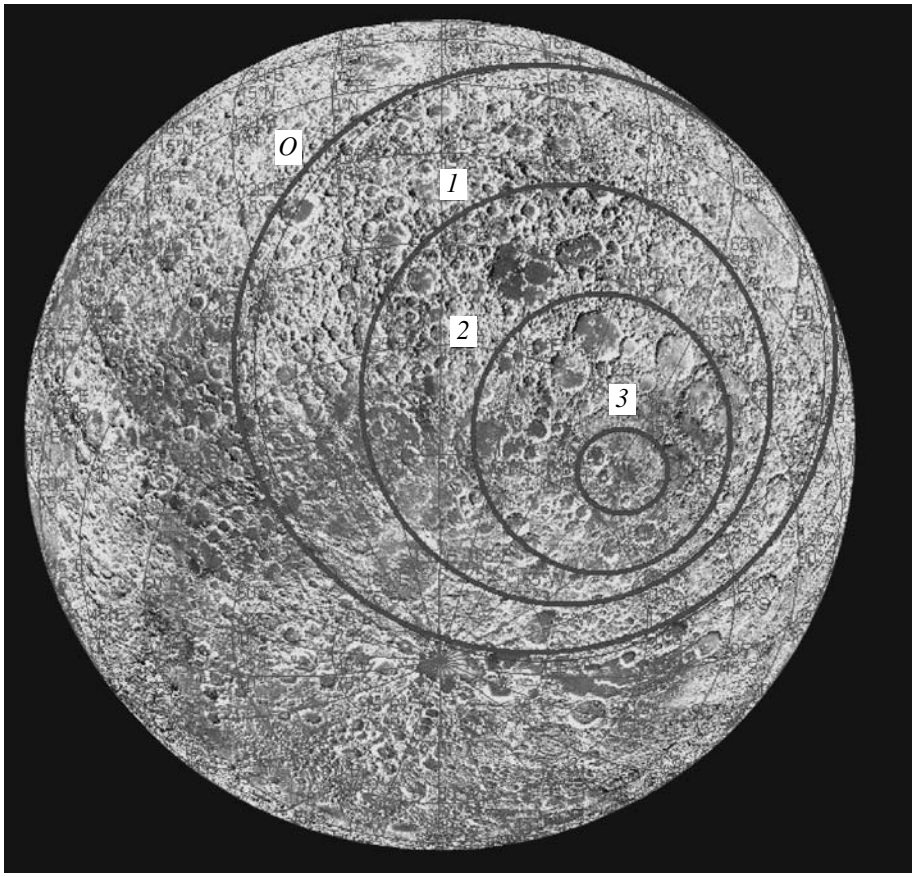

Fig. 16. The distinguished rings of the SPA basin structure overlapped (for obvious reasons) on an image of the Moon in the oblique orthographic projection with the 160°E central meridian.

conditionally corresponds to the boundary of the first inner ring.

In the presented model of the basin hypsometric structure, the rings of the basin inner depression have the shape of megaterraces. The ellipses presented in Fig. 16 show the position of the statistically distinguished boundary of transition from one level to another.

Ring *1* in Fig. 16 has a clearly defined elliptic shape with the center shifted southeastward from the outer ring center. The major semiaxis of the above ellipse is ~970 km. The average iron abundance below the first ring (4.0–5.5% Fe) corresponds to the characteristics of the breccia samples delivered from the *Apollo-16* (3.88% Fe) and *Luna-20* (5.81% Fe) moon-landing sites (Haskin and Warren, 1995), i.e., to typical continental samples of predominantly anorthosite rocks. The same conclusion is confirmed by comparing the thorium content (1.5–2.0 ppm Th). Thus, we can conclude that the considered zone of the impact structure is located within the upper lunar crust.

Ring *2* in Fig. 16 also has the shape of an ellipse with a major semiaxis of ~640 km as measured along the spherical surface. The center of this ellipse is shifted even further southeastward from the outer ring center.

The surface rock chemistry below ring *2* is characterized by the average iron and thorium abundances higher than 5.5% and 2.5 ppm, respectively. Proceeding from these data, we can conclude that the rocks have been insignificantly carried from the middle and lower crust to the surface in the considered depression zone.

The shape of the third distinguished ring is the closest to a circle with a radius of about 210 km. The center of this ring has been shifted by ~730 km from the outer ring center in the same southeastern direction.

The elliptic shape of the inner rings of the SPA basin structure was independently confirmed by Garrick-Bethell (2004), who used a technique similar to the procedure of the combined analysis applied in the present work.

The map in Fig. 16 demonstrates a high degree of degradation of the SPA basin inner regions as a result of numerous later impact events. According to different estimates, the SPA basin age varies from 4.1 to 3.9 Ga (Petro and Pieters, 2002; Warren, 2003; Jolliff et al., 2003), although an even earlier epoch (4.3–4.5 Ga) appears in certain publications (Schmidt, 2001; Peterson et al., 2002; Warren, 2003). In this case, some researchers note that the age of a special cluster of impact breccia, distinguished from the samples deliv-

ered on Earth, corresponds to 3.7–3.9 Ga, which can identify an epoch of increased intensity of lunar surface bombardment by different-origin impactors (Schmitt, 2001; Warren, 2003). A comparative analysis performed by Kring and Cohen (2002) also indicates that the period of an anomalously intense bombardment of the surface of bodies in the inner part of the Solar System was from 3.9 to 4.0 Ga ago, i.e., during the first 500–600 Myr after the completion of the Moon accretion stage.

At the same time, a thorough remote analysis of the surface regolith leads to the conclusion that about 75% of the observed rocks belong to an abyssal matter once carried on the surface and modified during the process of subsequent regolith formation (Pieters et al., 2001; 1997; Petro and Pieters, 2004).

On the other hand, a low thorium content of the rocks in the deepest zone of the present-day SPA basin depression can confirm the assumption that the initial penetration of the impact structure was relatively shallow and did not reach the middle crust (Jolliff et al., 2002). This conclusion quite agrees with the character of the thorium distribution within the SPA basin structure shown in Fig. 12. Within ring *2* (Fig. 16), thorium is distributed evidently asymmetrically and the distribution configuration is characterized by an anomaly in the northwestern sector. As mentioned above, the data obtained by us confirm that a material enriched in thorium could be carried from outside (Wieczorek and Zuber, 2001; Petro and Pieters, 2004; Garrick-Bethell and Zuber, 2005), rather than these rocks being directly related to an abyssal mafic matter. The interpretation of the data on the FeO and Th abundances, obtained based on the Clementine measurements applied to the SPA basin region, also agrees with similar conclusions (Lawrence et al., 2003).

On the contrary, an increased thorium content was not observed within ring *3*, which belongs to the deepest (to –8.5 km) zone of the SPA basin (Fig. 12).

We should add to the aforesaid that the basin structure was not substantially changed as a result of viscous relaxation during the prolonged period of post-impact metamorphism (Hiesinger and Head, 2004) and does not show indications of the following change in the total depression depth as compared to the initial shape.

Thus, these data also confirm the above conclusion that the central depression of the observed impact structure was also anomalously shallow in the primary state as compared to the depression diameter. This circumstance of exclusive significance for the SPA structure is especially evident when the profiles constructed on the spherical basis (Figs. 3, 4, and 6) are analyzed, even when taking into account that the vertical scale of the last two profiles is increased by a factor of 20.

Close analogs are also absent among classical models of the origin and evolution of multiring basins (Melosh, 1989). The model of megaterraces, which is outwardly most similar to the SPA basin structure (Head, 1974, 1977), cannot be applied simply because the inner ring system of the Mare Orientale, used as the basis for this model, has a strictly centrally symmetrical structure in contrast to the SPA basin system.

Certain elements of the model of the shock-wave process in the mega-layered medium can possibly be used to solve the problem of the origin of the SPA basin's unique structure in connection with the formation of multiring basins (Shevchenko et al., 1986). In this case, we can apparently consider the upper crust horizons, taking into account their differentiation indicated in accordance with the chemistry–depth dependence. However, this problem requires an additional and more detailed study.

DISCUSSION OF THE RESULTS

The SPA basin structure differs from other similar formations on the Moon. A comparison of the chemical characteristics of the bottom matter with the height levels of the matter's predominant concentration confirms the result of the hypsometric analysis of this structure.

An important feature of the proposed model of this ring structure consists in that the arrangement of the basin inner rings differs from the central circular symmetry.

A similar feature is possibly typical of lunar megabasins. According to the reconstruction of the ancient multiring structure, including Oceanus Procellarum, Mare Imbrium, Mare Serenitatis, and Mare Tranquillitatis, three distinguished inner rings are shifted northward (Whitaker, 1980). Byrne (2006) confirmed the existence of a similar megabasin (the term proposed by the author of this work) and indicated that the shape of this megabasin corresponds to an ellipse with its major axis oriented in the east–west direction.

One of the first indications that the rings in the SPA basin inner depression are shifted in the north–south direction was in Wood and Gifford (1980). As a result of the analysis of the global lunar topography, Byrne (2006) also found that the SPA basin rings differ from the centrally symmetrical configuration and are shifted in the north–south direction. A recent model of the SPA basin general structure (Garrick-Bethell, 2004) indicates that three conditional ellipses distinguished by this author are shifted southeastward at an angle of 85°–75° with respect to the equatorial plane.

The results reported in the present work comprehensively confirm that such a model of the basin structure is real since a systematic clearly defined shift of the centers of individual rings southeastward from the outer ring center was revealed based on an independent analysis of the hypsometric characteristics and on the specific distribution of iron and thorium.

Several researchers (Schultz and Gaut, 1990; Schultz and Anderson, 1996; Schultz, 1997; Wieczorek et al., 1999; Garrick-Bethell, 2004) assume that a similar difference in the large ring currents from the central

symmetry can be caused by an oblique impact of an impactor with respect to the local vertical.

Specifically, Schultz (1997) assumed that an anomalously shallow excavation depth at a large diameter of the SPA basin can be explained by a low impact velocity (lower than 5 km/s), by a low impactor density (less than 2 g cm^{-3}), or by an oblique impact (the impact trajectory inclination with respect to the horizon is lower than 30°). When Wieczorek and Phillips (1999) considered the difference in the depth–diameter ratio of the SPA basin from the tendency observed for other large lunar ring structures, they assumed that the effect of oblique impact could increase with increasing dimensions of the impactor.

The shift direction of the secondary ring centers obtained in the present work makes an angle of about 75° with the lunar equatorial plane (or the ecliptic plane, which is the same in the first approximation). Based on the assumption that this shift resulted from an oblique impact of an impactor that produced the SPA basin, it is not improbable that this direction can be interpreted as a trace of the impactor trajectory immediately before contact with the lunar surface.

These assumptions completely agree with the main results obtained by Garrick-Bethell (2004).

CONCLUSIONS

Without going into the details of the impact process simulation, we can refer to two probable assumptions. A hypothetical impactor followed a trajectory (or orbit) oriented almost normally to the ecliptic plane (1). Long-period comets or the Kuiper Belt objects, which are possibly the same, are among the known large objects with such orbits. Since past asteroids or planetesimals had orbits close to the ecliptic plane (or to the preplanet disk plane) (Dorofeeva and Makalkin, 2004), this considerably decreases the probability of an SPA basin origin due to the impact of a similar body.

Byrne (2005, 2006) directly indicated that an impactor that produced the SPA basin and belonged to the population of bodies different from impactors that caused all other basins on the Moon.

O'Keef and Ahrens (1982) indicated that a decrease in the depth–diameter ratio in impact structures results from a decrease in the impactor matter density, other conditions being equal. As mentioned above, Schultz (1997) also assumed that a low impactor density can be one of the causes of an anomalously small depth–diameter ratio. Certain problems stemming from this theory were considered by Shevchenko (1999) as applied to the conditions of impact structure formation on the Moon. Taking these data into account, we can assume that the impactor that produced the SPA basin excavation depression also had a low density (2 g/cm^3).

Proceeding from these two statements, we can make the hypothetical conclusion that the unique features of the SPA basin's nature can be caused by the unusual basin formation as a result of the impact of a comet-type body.

At the same time, it is very popular to classify the nature of the Kuiper Belt bodies as nuclei of inactive large comets. The estimated number of trans-Neptunian objects is very large. However, the position of these objects at the Solar System periphery generally limits the total mass of these objects, which results in the conclusion that the average density of the considered objects is extremely low.

The predominance of the Kuiper Belt objects or gigantic comet bodies from the Oort cloud among the main types of impactors during the assumed period of the SPA basin origin is justified in several works (see, e.g., Morbidelli, 1997, 1998; Murray and Holman, 1999; Fernandez and Gallardo, 1999; Schmitt, 2001).

ACKNOWLEDGMENTS

The authors are grateful to A.T. Basilevsky and Yu.A. Nefed'ev for useful discussions of the paper and very valuable comments.

REFERENCES

Byrne, C.J., Size Distribution of the Lunar Basins, *Lunar and Planet. Sci. Conf. XXXVI*, 2005, Abstract #1260.

Byrne, C.J., The Near Side Megabasin of the Moon, *Lunar and Planet. Sci. Conf. XXXVII*, 2006, Abstract #1930.

Chikmachev, V.I., Relief of the Far Side of the Moon in the Path of the *Zond-8* Probe, *Izv. Vyssh. Uchebn. Zaved., Geodez. Aerofotos"emka*, 1983, no. 1, pp. 97–99.

Chikmachev, V.I., Results of Analog Processing of Zond-Probe Photographs, *Aspects of the Complex Investigation of the Moon*, Shevchenko, V.V., Ed., Moscow: Mosk. Gos. Univ., 1986, pp. 42–56.

Chikmachev, V.I. and Shevchenko, V.V., A Macromodel of the Lunar South-Pole-Region Relief, *Astron. Vestn.*, 1999, vol. 33, no. 2, pp. 18–28 [*Sol. Syst. Res.* (Engl. Transl.), vol. 33, no. 2, p. 15].

Chikmachev, V.I., Pugacheva, S.G., and Shevchenko, V.V., General Structure of the Lunar South Pole - Aitken Basin and Possible Genesis of It, *Lunar and Planet. Sci. Conf. XXXVI*, 2005, Abstract #1078.

Dorofeeva, V.A. and Makalkin, A.B., *Evolyutsiya rannei Solnechnoi sistemy* (Evolution of the Early Solar System), Moscow: Editorial URSS, 2004.

Fernandez, J.A. and Gallardo, T., From the Oort Cloud to Halley-Type Comets, *Proc. IAU Coll. 173: Evolution and Source Regions of Asteroids and Comets*, Svoren, J., et al., Ed., 1999, pp. 327–338.

Garrick-Bethell, I., Ellipses of the South Pole - Aitken Basin: Implications for Basin Formation, *Lunar and Planet. Sci. Conf. XXXV*, 2004, Abstract #1515.

Garrick-Bethell, I. and Zuber, M.T., An Indigenous Origin for the South Pole - Aitken Basin Thorium Anomaly, *Lunar and Planet. Sci. Conf. XXXVI*, 2005, Abstract #2372.

Haskin, L. and Warren, P., Lunar Chemistry, *Lunar Sourcebook*, Heiken, G., Vaniman, D.T., and French, B.M.,

Eds., Houston: Cambridge Univ. Press, 1995, pp. 357–474.

Head, J.W., Orientale Multi-Ringed Basin Interior and Implications for the Petrogenesis of Lunar Highland Samples, *The Moon*, 1974, vol. 11, pp. 327–356.

Head, J.W, Origin of Outer Rings in Lunar Multi-Ring Basin. Evidence from Morphlogy and Ring Spacing, *Impact and explosion cratering*, Roddy, D.J., Pepin, R.O., and Merrill, R.B., Eds., New York: Pergamon, 1977, pp. 563–573.

Hiesinger, H. and Head, J.W.., Lunar South Pole - Aitken Impact Basin: Topography and Mineralogy, *Lunar and Planet. Sci. Conf. XXXV*, 2004, Abstract #1164.

Jolliff, B.L., Gillis, J.J., and Haskin, L.A., Eastern Basin Terrane and South Pole-Aitken Basin Ejecta: Mid-Level Crust?, *Lunar and Planet. Sci. Conf. XXXIII*, 2002, Abstract #1157.

Jolliff, B.L., Haskin, L.A., Korotev, R.L., *et al.*, Scientific Expectations from a Sample of Regolith and Rock Fragments from the Interior of the Lunar South Pole - Aitken Basin, *Lunar and Planet. Sci. Conf. XXXIV*, 2003, Abstract #1989.

Jolliff, B.L. and Gillis, J.J., South Pole - Aitken Basin and the Composition of the Lunar Crust, *Proc. 68th Annual Meteoritical Society Meeting*, 2005, Abstract #5330.

Kaula, W.M., Schubert, G., Lingenfelter, R.E., et al., Lunar Topography from Apollo 15 and 16 Laser Altimetry, *Proc. Fourth Lunar Sci. Conf.*, 1973, vol. 3, pp. 2811–2819.

Kislyuk, V.S., *Geometricheskie i dinamicheskie kharakteristiki Luny* (Geometric and Dynamic Characteristics of the Moon), Kiev: Naukova Dumka, 1988.

Kring, D.A. and Cohen, B.A., Cataclysmic Bombardment Throughout the Inner Solar System 3.9-4.0 Ga, *J. Geophys. Res., Ser. E*, 2002, vol. 107, no. 2, p. 5009. DOI: 10.1029/2001JE001529.

Ksanfomality, L.V., A Huge Basin in the Unknown Portion of Mercury in the 250°–290° W Longitude Range, *Astron. Vestn.*, 2004, vol. 38, no. 1, pp. 23–30 [*Sol. Syst. Res.* (Engl. Transl.), vol. 38, no. 1, pp. 21–27].

Lawrence, D.J., Feldman, W.L., Barraclough, B.L., et al., Global Elemental Maps of the Moon: The *Lunar Prospector* Gamma-Ray Spectrometer, *Science*, 1998, vol. 281, pp. 1484–1489.

Lawrence, D.J., Feldman, W.L., Elphic, R.C., et al., Iron Abundances on the Lunar Surface As Measured by the *Lunar Prospector* Gamma-Ray and Neutron Spectrometers, *J. Geophys. Res., Ser. E*, 2002, vol. 107, no. 12, p. 5130.

Lawrence, D.J., Pieters, C.M., Elphic, R.C., et al., Regional Elemental Abundances within South Pole - Aitken Basin As Measured with Lunar Prospector Gamma-Ray Spectrometer Data, *Lunar and Planet. Sci. Conf. XXXIV,* 2003, Abstract #1679.

Leikin, G.A. and Sanovich, A.N., Origin of the Southern Basin on the Far Side of the Moon, *Astron. Vestn.*, 1985, vol. 19, no. 2, pp. 113–119 [*Sol. Syst. Res.* (Engl. Transl.) vol. 19, no. 2, pp. 74–78].

Lucey, P.G., Taylor, G.J., Hawke, B.R., and Spudis, P.G., FeO and TiO2 Concentrations in the South Pole - Aitken Basin: Implications for Mantle Composition and Basin Formation, *J. Geophys. Res.,* 1998, vol. 103, pp. 3701–3708.

Lunar Prospector Reduced Spectrometer Data - Special Products, http://pds-geosciences.wustl.edu/missions/lunarp/rediced_special.html.2006.

Melosh, H.J., *Impact Cratering: A Geologic Process*, New York: Oxford Univ. Press, 1989. Translated under the title *Obrazovanie udarnykh kraterov: geologicheskii protsess*, Moscow: Mir, 1994.

Morbidelli, A., Chaotic Diffusion and the Origin of Comets from the 2/3 Resonance in the Kuiper Belt, *Icarus*, 1997, vol. 127, no. 1, pp. 1–12.

Morbidelli, A., New Insights on the Kuiper Belt, *Science*, 1998, vol. 280, no. 5372, pp. 2071–2073.

Murray, N. and Holman, M., The Origin of Chaos in the Outer Solar System, *Science*, 1999, vol. 283, no. 5409, pp. 1877–1881.

Nefed'ev, A.A., Maps of Relief of the Edge Zone of the Moon at the General Zero Level, *Izv. Astron. Obs. im. V.P. Engel'gardta*, 1958, no. 30.

O'Keef, J.D. and Ahrens, T.J., Cometary and Meteorite Swarm Impact on Planetary Surfaces, *J. Geophys. Res., Ser. B*, 1982, vol. 87, no. 8, pp. 6668–6680.

Peterson, C.A., Hawke, B.R., Blewett, D.T., et al., Geochemical Units on the Moon: The Role of South Pole-Aitken Basin, *Lunar and Planet. Sci. Conf. XXXIII*, 2002, Abstract #1601.

Petro, N.E. and Pieters, C.M., Reconstructing the Stratigraphy of the Ancient South Pole - Aitken Basin Interior, *The Moon beyond 2002: Next Steps in Lunar Science and Exploration*, 2002, no. 1, p. 47.

Petro, N.E. and Pieters, C.M., Surviving the Heavy Bombardment: Ancient Material at the Surface of South Pole - Aitken Basin, *J. Geophys. Res., Ser. E*, 2004, vol. 109, p. 06004.

Petro, N.E. and Pieters, C.M., The Effect of Basin Formation on the Lunar Geochemical Terranes, *Lunar and Planet. Sci.Conf. XXXVII*, 2006, Abstract #1868.

Pieters, C.M., Tompkins, S., Head, J.W., and Hess, P.C., Mineralogy of the Mafic Animaly in the South Pole - Aitken Basin: Implications for Excavation of the Lunar Mantle, *Geophys. Res. Lett.*, 1997, vol. 24, no. 15, pp. 1903–1906.

Pieters, C.M., Head, J.W., Gaddis, L., Jolliff, B., and Duke, M., Rock Types of South Pole-Aitken Basin and Extent of Basaltic Volcanism, *J. Geophys. Res.*, 2001, vol. 106, pp. 28001–28022.

Pike, R.J. and Spudis, P.D., Basin-Ring Spacing on the Moon, Mercury, and Mars, *Earth, Moon, Planets*, 1987, vol. 39, pp. 129–194.

Rodionov, B.N., Nefed'ev, A.A., Shpekin, M.I., et al., Study of Topography of the Far Side of the Moon on the Basis of *Zond-8* Photographs, *Kosm. Issled.*, 1976, vol. 14, no. 4, pp. 624–629.

Schultz, P.H., Forming the South Pole - Aitken Basin: The Extreme Games, *Lunar and Planet. Sci. Conf. XXVIII,* 1997, Abstract #1787.

Schultz, P.H. and Anderson, R.R., Asymmetry of the Manson Impact Structure: Evidence for Impact Angle and Direction, *Geol. Soc. Am. Spec. Paper*, 1996, vol. 302, pp. 397–417.

Schultz, P.H. and Gault, D.E., Prolonged Global Catastrophes from Oblique Impacts, *Geol. Soc. Am. Spec. Paper*, 1990, vol. 247, pp. 239–261.

Shevchenko, V.V., On the Cometary Origin of the Lunar Ice, *Astron. Vestn.*, 1999, vol. 33, no. 5, pp. 456–465 [*Sol. Syst. Res.* (Engl. Transl.), vol. 33, no. 2, p. 400].

Shevchenko, V.V., Leikin, G.A., and Sanovich, A.N., On the Origin of Multiring Basins, *Aspects of the Complex Investigation of the Moon*, Shevchenko, V.V., Ed., Moscow: Mosk. Gos. Univ., 1986, pp. 71–80.

Shevchenko, V.V., Sanovich, A.N., and Lejkin, G.A., On Problem of Origin of Multirings Basin, *Lunar and Planet. Sci. Conf. XVI*, 1985, pp. 775–776.

Schmitt, H.H., Source and Implications of Large Lunar Basin-Forming Objects, *Lunar and Planet. Sci. Conf. XXXI*, 2001, Abstract #1821.

Spudis, P.D., *The Geology of Multi-Ring Impact Basins*, New York: Cambridge Univ. Press, 1993.

Spudis, P.D., Reisse, R.A., and Gillis, J.J., Ancient Multiring Basin and the Moon Revealed by *Clementine* Laser Altimetry, *Science*, 1994, vol. 266, pp. 1848–1851.

Stuart-Alexander, D.E., Geologic Map of the Central Far Side of the Moon, Scale 1:5000000, *U. S. Geol. Surv. Bull.*, 1978, I-1047.

Warren, P.H., Lunar Prospector Data Imply An Age of 4.1 Ga for the Nectaris Basin, and Other Problems with the Lunar "Cataclysm" Hypothesis, *Large Meteorite Impacts*, Houston: LPI Publ., 2003, p. 4129.

Whitaker, E.A, The Lunar Procellarum Basin, *LPI Contribution 414*, Merrill, R.B. and Schultz, P.H., Eds., Houston: LPI Publ., 1980, pp. 101–103.

Wieczorek, M.A. and Phillips, R.J., Lunar Multiring Basins and the Cratering Process, *Icarus*, 1999, vol. 139, pp. 246–259.

Wieczorek, M.A. and Zuber, M.T., A Serenitatis Origin for the Imbrian Grooves and South Pole-Aitken Thorium Anomaly, *J. Geophys. Res.,* 2001, vol. 106, p. 864.

Wilhelms, D.E., The Geologic History of the Moon, *U. S. Geol. Surv. Prof. Pap.*, 1987, 1348.

Wilhelms, D.E., et al., Geological Map of the South Side of the Moon, Scale 1:5000000, *U. S. Geol. Surv. Misc. Invest. Ser.*, 1979, I-1162.

Wood, C.A. and Gifford, A.W., Evidence for the Lunar Big Backside Basin, *Conference on Multi-Ring Basins: Formation and Evolution, LPI Contribution 414*, Merrill, R.B. and Schultz, P.H., Eds., Houston: LPI Publ., 1980, pp. 121–123.